Evaluation of Structure-Function Relationships in Asthma using Multidetector CT and Hyperpolarized He-3 MRI[1]

Sean B. Fain, PhD, Guillermo Gonzalez-Fernandez, MS, Eric T. Peterson, MS, Michael D. Evans, MS
Ronald L. Sorkness, PhD, Nizar N. Jarjour, MD, William W. Busse, MD, Janet E. Kuhlman, MD

Rationale and Objectives. Although multiple detector computed tomography (MDCT) and hyperpolarized gas magnetic resonance imaging (HP MRI) have demonstrated ability to detect structural and ventilation abnormalities in asthma, few studies have sought to exploit or cross-validate the regional information provided by these techniques. The purpose of this work is to assess regional disease in asthma by evaluating the association of sites of ventilation defect on HP MRI with other regional markers of airway disease, including air trapping on MDCT and inflammatory markers on bronchoscopy.

Materials and Methods. Both HP MRI using helium-3 and MDCT were acquired in the same patients. Supervised segmentation of the lung lobes on MRI and MDCT facilitated regional comparisons of ventilation abnormalities in the lung parenchyma. The percentage of spatial overlap was evaluated between regions of ventilation defect on HP MRI and hyperlucency on MDCT to determine associations between obstruction and likely regions of gas trapping. Similarly, lung lobes with high defect volume were compared to lobes with low defect volume for differences in inflammatory cell number and percentage using bronchoscopic assessment.

Results. There was significant overlap between sites of ventilation defect on HP MRI and hyperlucency on MDCT suggesting that sites of airway obstruction and air trapping are associated in asthma. The percent ($r = 0.68$; $P = .0039$) and absolute ($r = 0.61$; $P = .0125$) number of neutrophils on bronchoalveolar lavage for the sampled lung lobe also directly correlated with increased defect volume.

Conclusions. These results show promise for using image guidance to assess specific regions of ventilation defect or air trapping in heterogeneous obstructive lung diseases such as asthma.

Key Words. Asthma; functional imaging; lungs; hyperpolarized gas; MRI; MDCT.

Asthma affects millions of people worldwide and trends indicate increasing incidence, especially in children (1,2). Subjects with asthma experience periodic wheezing and shortness of breath that manifests on pulmonary function tests as reduced forced expiratory lung volume in 1 second (FEV_1) and increased lung residual volume normalized to the total lung capacity (RV/TLC) compared with normal subjects. Bronchodilation with beta agonists such as albuterol can partially reverse this obstructive physiology by relaxing airway smooth muscle, but evidence from airway biopsies sug-

Acad Radiol 2008; 15:753–762

[1] Departments of Medical Physics (S.B.F.), Biomedical Engineering (S.B.F., E.T.P.), Electrical and Computer Engineering (G.G.-F.), Biostatistics and Medical Informatics (M.D.E.), Morris Institute for Respiratory Research (R.L.S., N.N.J., W.W.B.), and Medicine (N.N.J., W.W.B.), University of Wisconsin, Madison, WI; Department of Radiology, J5/M158 CSC, University of Wisconsin Hospital, University of Wisconsin, Madison, WI 53792 (S.F.B., J.E.K.). Received August 2, 2007; accepted October 17, 2007. **Address correspondence to:** S.B.F. e-mail: sfain@wisc.edu

doi:10.1016/j.acra.2007.10.019

gests that obstruction is also accompanied by chronic inflammation and airway remodeling (3).

Functional imaging in the lungs has great potential for mechanistic studies of lung disease, particularly for identifying regional patterns of obstruction that test physiologic hypotheses (4–7). Regional mosaics of reduced parenchymal density, apparently from air trapping, are associated with asthma on computed tomography (CT) (8). More recently, CT, and especially multidetector CT (MDCT), have been used to quantitatively measure lung parenchymal density and correlate these measures to obstructive physiology (9,10).

Regional patterns of ventilation in asthma have also been explored using inhaled gas contrast agents in conjunction with imaging (11–14), including hyperpolarized helium-3 magnetic resonance imaging (HP MRI) (15). Just as MDCT measures of parenchymal density, whole lung measures of ventilatory defect number on HP MRI correlate with obstructive physiology (7,14,16). Recently, a substantial fraction of the regions of ventilation defect were shown to persist on repeated HP MRI studies of asthma patients separated in time by 1 week to more than 1 year (16). Similarly, whole lung images of ventilation acquired with HP MRI can be used to localize and quantify the percentage of ventilation defect over the whole lung (17) and potentially by lung lobe. Structure and function assessment of parenchymal density near regions of ventilation defect is therefore possible by combining the MDCT and HP MRI techniques.

The pathogenesis of airway obstruction in asthma involves smooth muscle hyperreactivity, inflammation and airway remodeling. Several studies suggest spatially heterogeneous patterns of ventilation that may be driven by local differences in structure and function. The hypothesis of this work is that imaging can provide a means to guide regional assessment of airway abnormalities to better identify regions of more intense disease in the lungs. Imaging can therefore provide a valuable tool to better assess mechanisms and distinguish different phenotypes of obstructive lung disease. Data from HP MRI and MDCT of the lungs in the same subjects with mild to moderate and severe asthma are compared with whole lung measures of physiology and with each other to explore the spatial correspondence of features of air trapping, ventilation defect, and inflammation.

MATERIALS AND METHODS

Our study was approved by our Institutional Review Board and was compliant with the Health Insurance Portability and Accountability Act. The inhalation of hyperpolarized ^{3}He gas for MRI is regulated as NC100182. Our studies were conducted under an investigational new drug (IND #64,687) protocol approved by the Food and Drug Administration. A total of 45 subjects with asthma (29 $\pm$ 10 years; 19 males and 26 females) underwent MDCT of the lungs at two different lung volumes: full inspiration and at end-expiration, corresponding to TLC and functional residual capacity (FRC), respectively. These subjects were included in the study based on history of asthma using the criteria set forth by the expert panel of the National Institutes of Health (18), including reversibility of 12% or greater (at least 200 mL) after bronchodilation or methacholine reactivity with a provocative concentration causing a 20% decrease in FEV_1 (PC20) of <8 mg/mL. Exclusion criteria included upper respiratory infection within 2 weeks, >5 pack years of smoking history, or a smoker in the past year. If a subject had previously smoked, a diffusion capacity was measured to ensure that it was $>70\%$ predicted. For added safety from concerns about inhalation of the anoxic $^3He/N_2$ gas mixture, subjects were excluded from HP MRI if their percentage of FEV_1 % predicted was less than 60%.

A subset of 21 of 45 (47%) subjects (30 $\pm$ 11 years; 9 males and 12 females) who underwent MDCT were also imaged with HP MRI and were analyzed for severity of *regional* ventilation defects and their correspondence to regions of focal air trapping on MDCT. Six of these 21 (29%) subjects were further characterized as severe asthmatics based on the criteria set forth in the Severe Asthma Research Program (19)—these include as a chief criterion the prolonged use of high dose corticosteroids to control symptoms (>880 μg).

Pulmonary Function and Bronchoscopy

Spirometry and plethysmographic lung volume measurements were performed in all subjects according to American Thoracic Society/European Respiratory Society guidelines (20,21). Subjects withheld short-acting beta agonist treatments for 4 hours, long-acting beta agonist treatments for 12 hours, and other bronchodilator medications for an appropriate length of time to avoid interference with the measurements. The FEV_1 acquired immediately before MRI was used as the subject's baseline FEV_1 for analysis in all cases. Predicted values for FEV_1, forced vital capacity, FEV_1/forced vital capacity ratio, and forced expiratory flow rate at 25–75% forced vital capacity were computed using the equations of Hankinson et al (22). Predicted values for TLC, FRC, FRC/TLC ratio, resid-

ual volume (RV), and RV/TLC ratio were computed using the equations of Stocks and Quanjer (23), with adjustments for African Americans per American Thoracic Society recommendations (24). Plethysmography measures were acquired 1–4 weeks before HP MRI.

Bronchoscopic assessment was performed in 16 of 21 (76%) subjects within 1 week of imaging. Bronchoalveolar lavage (BAL) was acquired in a specific lobe, usually the right middle or right upper lobe, and inflammatory cell markers; including absolute and percent neutrophils, eosinophils, and macrophages; were retrospectively compared with the percentage of defect volume for the sampled lobe.

Image Acquisition

MRI and MDCT acquisitions were performed within 48–72 hours of each other. Bronchoscopy was performed within 1 week of the last imaging study, usually CT. The time varied because of the logistical challenges of reconciling subjects' schedules with clinical openings and scanner availability.

In all subjects, MDCT imaging was performed using a GE Light Speed CT scanner with 16 or 64 detectors (GE Medical Systems, Milwaukee, WI). Three scans were acquired, each in a breath-hold of ~4 seconds: a low-resolution scout scan followed by two high-resolution scans, one at TLC followed by one at FRC. Two three-dimensional lung volumes were then reconstructed, one at 0.625-mm slice thickness for quantitative measurement at nearly isotropic voxel size and one at 5-mm slice thickness for qualitative evaluation and registration to MRI. Other specific acquisition and reconstruction parameters used for MDCT data were as summarized in Table 1.

MRI was performed using a 1.5 T MR scanner with broadband capabilities (Signa LX, GE Medical Systems). MRI for each subject included two conventional proton scans using the system's body radiofrequency (RF)-coil: a T1-weighted scout localizer followed by a single shot two-dimensional multislice fast spin echo breath-held acquisition in the axial plane with field of view, slice thickness, and position matching the subsequent HP MRI scan. Before the fast spin echo acquisition, the subject inhaled a volume of air equivalent to the volume of $^3He/N_2$ mixture to be inhaled to match the position of the diaphragm for both scans.

For the ^3He MRI scan, a helium polarizer (IGI.9600, GE Healthcare) located adjacent to the MRI scanner used the spin exchange optical pumping method to polarize ^3He to 30%–40%. The hyperpolarized gas contrast agent was a mixture of ^3He and N_2 with a net activity of polarized ^3He of 4.5 mM. The $^3He/N_2$ mixture was prepared by mixing 200–300 mL of 30%–40% polarized ^3He with nitrogen gas added to reach a total volume equivalent to 15% of the subject's TLC. This mixture was added to a Tedlar bag (Jensen Inert Inc, Coral Springs, FL) that had been purged and rinsed with nitrogen to remove oxygen. The polarized gas was inhaled by the subject through an attached 1/8-inch Tygon tube (US Plastic Corp, Lima, OH) starting with their lung volume at FRC.

A vest RF coil (IGC-Medical Advances, Milwaukee, WI) tuned to operate at the resonant frequency of ^3He and decoupled from the body RF-coil was used so that HP MRI and proton MRI could be acquired without moving the subject. A short 1- to 2-second scan was used in conjunction with a ~100 mL sip of ^3He to determine center frequency and flip angle using the method outlined elsewhere (25). The HP MRI ventilation acquisition consisted of a fast two-dimensional, multislice gradient recalled echo (GRE) breath-held acquisition in the axial plane with 128 × 128 acquired matrix. The slice number for both fast spin echo and HP MRI ranged between 13 and 19 slices to achieve whole lung (superior to inferior) coverage. Other specific imaging parameters are as summarized in Table 2. Electrocardiogram and oxygen saturation signals were monitored throughout the imaging session.

Table 1
Multidetector Computed Tomography Scan Parameters

Parameter	16 Detector	64 Detector
Collimation	1.25 mm	1.25 mm
Pitch	1.675	0.984
Source current/ voltage	50 mA/120 kVp	50 mA/120 kVp
Gantry speed	0.5 second/rotation	
Matrix	512 × 512	
Lung volume	Functional residual capacity (expiratory) and total lung capacity (inspiratory)	
Reconstruction kernel	"Standard" and "lung"	
Reconstructed slice thickness	0.625 mm (quantitative) and 5 mm (qualitative)	

Image Measurement

Whole lung air trapping on MDCT was quantitatively evaluated by calculating the percent of the lung volume falling below the thresholds of −850, −910, and −950 Hounsfield units on expiratory CT. Additionally, focal regions of hyperlucency on MDCT were scored according to size and percentage of spatial overlap with regional ven-

Table 2
Magnetic Resonance Imaging Scan Parameters

Parameter	T1-Weighted Fast Spin Echo	Hyperpolarized ^{3}He Magnetic Resonance Imaging
Repetition time/echo time	∞/8 milliseconds	8.4/3.1 milliseconds
Flip angle	90°	7°
Bandwidth	31.25 kHz	31.25 kHz
Acquisition matrix	128 × 64	128 × 128
Imaging time	7–8 seconds	18–24 seconds
Axial plane field of view	32–38 × 24–29 cm^2	
Slice field of view	13–19 × 1.5 cm slices	

tilation defects on HP MRI to test for similar regional patterns of air trapping and obstruction. The MRI and CT data were evaluated separately for size and location of ventilation defects on HP MRI and regions of hyperlucency based on the expiratory CT images, respectively. After identifying these regions, the radiologist then assessed their degree of overlap using a 4-point scale. The four-point scale assigned a value of 0 for no overlap, 1 for 26%–50% overlap, 2 for 51%–75%, and 3 if >75% overlap.

For whole lung comparisons to pulmonary function, a discrete score similar to that used elsewhere (14) was used to measure ventilation defect number on HP MRI. A radiologist (J.E.K.) evaluated the extent and location of defects by slice. If a defect was identified in a given slice, it was assigned a score based on its extent within that slice: 1 if ≤25%, 2 if between 26% and 50%, 3 if between 51% and 75%, and 4 if >75%. The total lung defect score was calculated by summing the score over each slice. The minimum defect score was therefore zero, but the maximum depended on the total number defects observed.

For regional comparisons, a quantitative and continuous measure of the percent defected volume (% defect volume) for each lung lobe was calculated in a manner similar to that described elsewhere (17). In contrast to previous studies, the defect volume was assessed for each lung lobe by displaying both MRI and inspiratory MDCT images for each subject in spatial registration (Fig 1a,b) in a graphic user interface (Fig 1c) written in Matlab 7.0 (The Mathworks, Natick, MA). The lung lobes and defect regions were segmented manually from the proton MRI and HP MRI images, respectively, by combining thresholding along with display of the lobe boundaries on MDCT images. This analysis resulted in a defect mask and a lobe volume mask that exploited the inherent spatial registration of the helium and proton MRIs to calculate the defect volume by simply multiplying the two masks and summing the result.

Statistical Analyses

The study design compared whole lung measures of ventilation defects on HP MRI and sites of hyperlucency on MDCT with pulmonary function measures of obstructive physiology. The volume and regional association of ventilation defects on HP MRI and sites of hyperlucency on MDCT were also compared on a whole lung and regional basis. The Spearman rank correlation was used to test for associations between image measures and pulmonary function measures. The Wilcoxon rank-sum test was used to measure differences between groups. McNemar's test was used to assess regional overlap of airway abnormalities on imaging.

RESULTS

No adverse events occurred during MRI studies. The oxygen saturation for all subjects remained higher than 90% in all cases, recovering to pre-^{3}He inhalation levels within 5–10 seconds after the end of the breath-hold. Pulmonary function measures using spirometry and plethysmography were not significantly different for severe versus nonsevere subjects included in this study. However, the FEV_1 % predicted (%p) tended to be lower in severe versus nonsevere subjects ($P = .055$) (Table 3). Significant correlations between image metrics and whole lung measures of pulmonary function are summarized in Table 4.

MDCT Measures

Densitometry for the −850 Hounsfield units threshold on expiratory CT correlated (Table 4) directly with RV/TLC%p ($r = 0.53$, $P = .003$), but this relationship did not hold for thresholds at −910 and −950. There was not significantly different densitometry for severe versus nonsevere subjects ($P = .61$) on MDCT (Table 3), but nor was there significantly different RV/TLC%p for these groups.

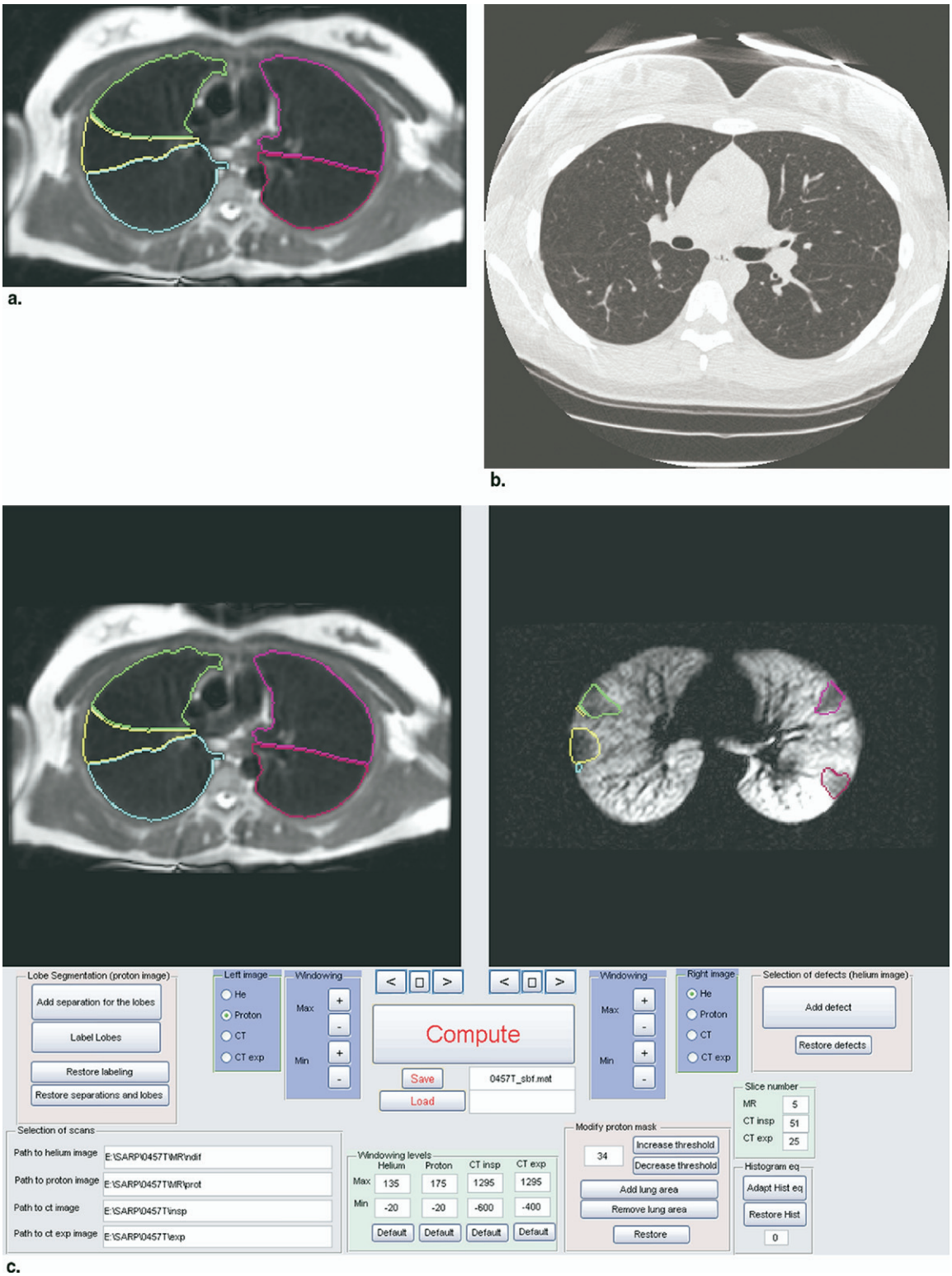

Figure 1. **(a)** Segmented lung lobes (color code: yellow: right middle lobe; green: right upper lobe; blue: right lower lobe; magenta: left upper lobe; red: left lower lobe) overlain on fast spin-echo (FSE) conventional proton magnetic resonance imaging (MRI) of the lung parenchyma acquired with the FSE sequence (Table 2). **(b)** Corresponding inspiratory multidetector computed tomography (MDCT) slice (a) used for segmenting the lung lobes in (a). MDCT image in (b) 512 × 512, reconstructed at 0.5-cm thickness, using parameters summarized in Table 1. **(c)** Graphic user interface display with equivalent proton MRI and hyperpolarized (HP) MRI slices with segmented lung lobes as described in (a). The HP MRI of ventilation in the right panel of (c) depicts ventilation defects segmented with lobe location marked using the same color code and was acquired with a gradient recalled echo (GRE) sequence and parameters summarized in Table 2.

Table 3
Statistical Summary (Mean ± Standard Deviation) of Image Metrics and Pulmonary Function with Asthma Severity for Subjects Included in the Regional Analysis

Parameter	Severe (n = 6)	Nonsevere (n = 15)	Overall (n = 21)
Defect score	16.7 ± 12.3	11.0 ± 9.5	12.6 ± 10.4
Percent defect volume (%)	7.6 ± 4.2	5.4 ± 4.5	6.0 ± 4.4
Expiratory densitometry:			
Percent below −850 HU	4.7 ± 2.1	8.0 ± 7.3	7.0 ± 6.4
Percent below −910 HU	0.9 ± 1.0	1.5 ± 1.7	1.3 ± 1.6
Percent below −950 HU	0.3 ± 0.5	0.4 ± 0.7	0.4 ± 0.6
FEV_1 (% predicted)	82.7 ± 11.1	91.5 ± 15.1	89.0 ± 14.3
$FEF_{25–75}$ (% predicted)	71.7 ± 36.3	69.4 ± 23.4	70.0 ± 26.8
FEV_1/FVC (% predicted)	94.4 ± 13.6	89.2 ± 8.6	90.7 ± 10.2
RV/TLC	0.323 ± 0.098	0.308 ± 0.052	0.312 ± 0.066
BAL			
% Neutrophils	0.86 ± 0.86	2.48 ± 2.93	2.01 ± 2.58
% Eosinophils	0.74 ± 0.73	0.63 ± 0.67	0.66 ± 0.67
% Macrophage	91.3 ± 2.9	85.5 ± 11.2	87.2 ± 9.8

HU: Hounsfield unit; FEV_1: forced expiratory volume in 1 second; $FEF_{25–75}$: forced expiratory flow rate at 25–75% FVC; FVC: forced vital capacity; RV: residual volume; TLC: total lung capacity; BAL: bronchoalveolar lavage.

MRI Measures

On HP MRI, the number of ventilation defects correlated inversely with FEV_1%p ($r = -0.76$, $P = .0002$). There was no significant difference in ventilation defect score for severe versus nonsevere subjects ($P = .54$).

Regionally, ventilation defect volume was larger in the right middle lobe compared to the right upper ($P = .002$) and right lower lobes ($P = .008$). Severe subjects showed a higher defect volume in the left lower lobe ($P = .02$) compared with nonsevere subjects. The % defect volume burden at the site of bronchoscopic assessment correlated directly with both absolute ($r = 0.61$; $P = .0125$) and percent neutrophil ($r = 0.68$; $P = .0039$) counts in the BAL, whereas whole lung measures of percent defect volume did not correlate significantly with BAL neutrophil number ($r = 0.30$; $P = .27$) or percentage ($r = 0.41$ $P = .11$). In addition, highly defected lobes (≥10% defect volume) also showed greater absolute ($P = .05$) and percentage ($P = .03$) neutrophils (Fig 2) compared with less defected lobes (<10% defect volume). There was no relationship between the total number or percentage of eosinophils or macrophages and the defect measures on MRI.

MDCT and MRI Comparison

HP MRI and MDCT defects were found to be related overall ($P = .04$) and specifically for the right upper lobe ($P = .003$), left upper lobe ($P = .03$), and right middle lobe ($P = .04$). A typical example in the left lower lobe is shown in Fig 3. Qualitatively, there was greater correspondence between HP MRI defects and MDCT defects in severe asthma subjects compared to nonsevere subjects (Fig 4).

DISCUSSION

This work evaluates the physiologic significance of two image metrics of obstructive lung disease that have been established in previous studies (8,9,14) to correlated with whole lung measures of airway obstruction and air trapping. In the present study, ventilation defects on HP MRI and hyperlucency on MDCT were also shown to correlate with whole lung measures of obstruction and air trapping, respectively. In addition, both image measures were found to be regionally associated, suggesting a possible shared mechanism underlying airway obstruction and air trapping. Moreover, inflammatory cell markers from BAL were shown to be elevated in lobes with a large defect volume percentage compared to lobes with low defect volume percentage, consistent with elevated inflammatory processes near locations of airway obstruction.

These regional relationships suggest that locations of air trapping and obstruction might correlate to regions of structural anomaly that make airways prone to collapse at lower lung volumes. Specifically, focal regions of hyperlucency suggestive of air trapping on CT were found to spatially

Table 4
Spearman Correlations Between Image, Pulmonary Lung Function, and BAL Measures

Parameter	Correlate					
	FEV_1 % Predicted	FEV_1/FVC % Predicted	FEF_{25-75} % Predicted	RV/TLC % Predicted	BAL % Neutrophils	BAL Total Neutrophils (10^6 cells)
Defect score (n = 21)	−0.76 P = .0002	−0.24 P = .31	−0.54 P = .03	0.58 P = .02	0.23 P = .17	0.06 P = .82
Expiratory densitometry (n = 45)						
Percent below −850 HU	−0.37 P = .04	−0.52 P = .02	−0.55 P = .002	0.53 P = .003	0.16 P = .54	0.18 P = .51
% Defect volume						
Whole lung (n = 21)	−0.57 P = .007	−0.23 P = .31	−0.43 P = .08	0.37 P = .15	0.41 P = .11	0.30 P = .27
@BAL site (n = 17)	—	—	—	—	0.68 P = .0039	0.61 P = .0125

HU: Hounsfield unit; FEV_1: forced expiratory volume in 1 second; FEF_{25-75}: forced expiratory flow rate at 25–75% FVC; FVC: forced vital capacity; RV: residual volume; TLC: total lung capacity; BAL: bronchoalveolar lavage.

Figure 2. Scatterplot of high and low defected lobes showing increased percentage of neutrophils (P = .03) in lobes sampled with bronchoalveolar lavage and greater than 10% defect volume compared with lobes with less than 10% defect volume.

overlap with regions of ventilation defect on MRI, suggestive that similar mechanical features of the airways in these regions may drive both abnormalities. For example, the lung volumes at image acquisition differ by ~1 L, ranging from FRC for the expiratory MDCT to ~1 L above FRC for the HP MRI data. By definition, ventilation defect regions on HP MRI presented with diminished intensity with respect to surrounding lung parenchyma. These regions only rarely demonstrate a complete absence of signal. Therefore the data suggest that, on average, ventilation defect regions above FRC on HP MRI represent partially obstructed airways that fully collapse at FRC resulting in air trapping in this study population. Finally, the defect burden in lung lobes corresponding to the site of BAL had higher total and percent neutrophils compared with less defected lobes, suggestive of increased inflammation at sites of increased airway obstruction.

For the image markers used in this study, there were no clear differences between severe and nonsevere asth-

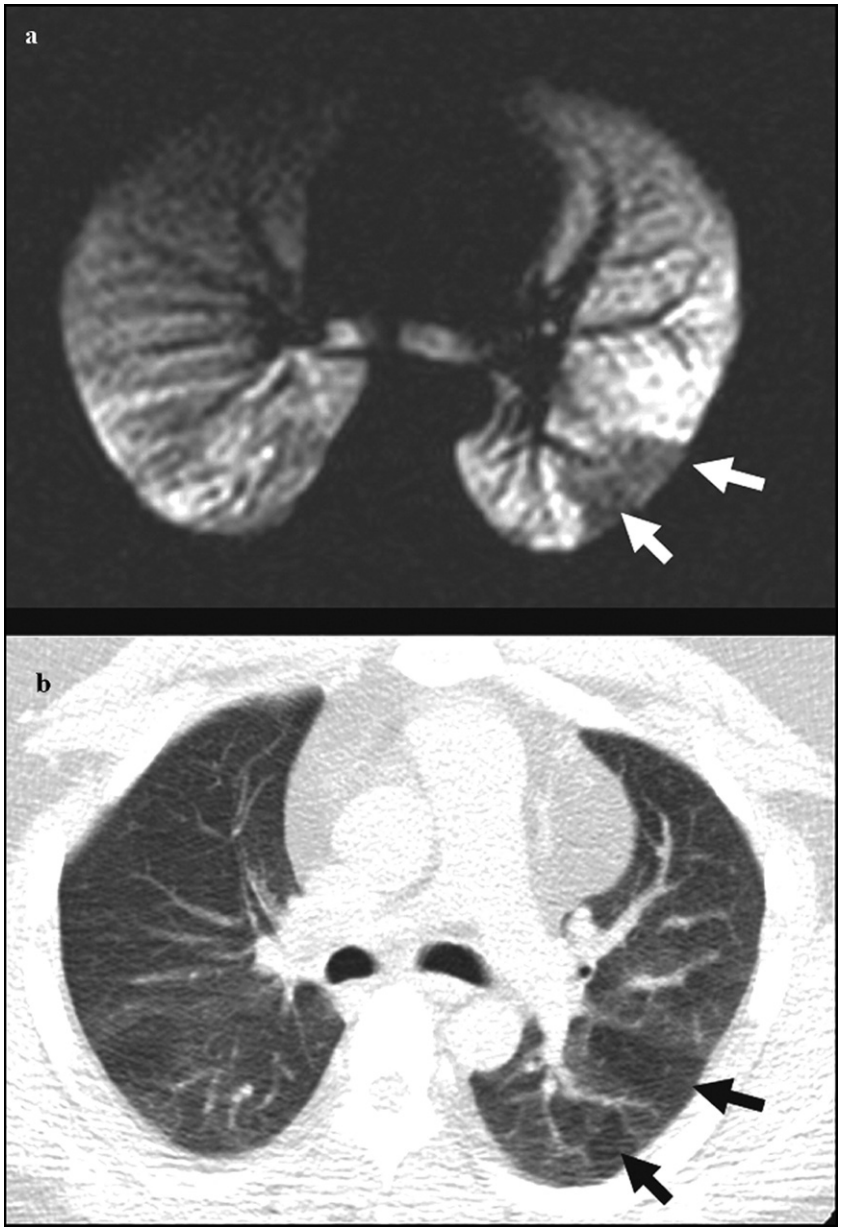

Figure 3. Typical example of the observed spatial correspondence **(a)** between ventilation defects on hyperpolarized (HP) magnetic resonance imaging (MRI) (white arrows) and **(b)** hyperlucency on multidetector computed tomography (MDCT) (black arrows). These defects in the left lower lobe reflect obstructive physiology at different lung volumes: 15% of total lung capacity for HP MRI in **(a)** and functional residual capacity for expiratory MDCT in **(b)**.

matics. This likely points to several limitations of the present study, including the small sample size and the exclusion criterion of FEV_1 <60%, which may have selected for a severe asthma population with minimal or modest baseline obstruction that is not necessarily representative of the severe asthma group in the Severe Asthma Research Program database. Also, although the MRI and CT images were read separately by the radiologist, they were read in succession, and thus the radiologist was not blinded to the previous analysis. A blinded, or preferably quantitative, analysis of spatial overlap would be more desirable. To address this limitation, a lobar segmentation of the expiratory MDCT data is being developed to more easily allow quantitative assessment of

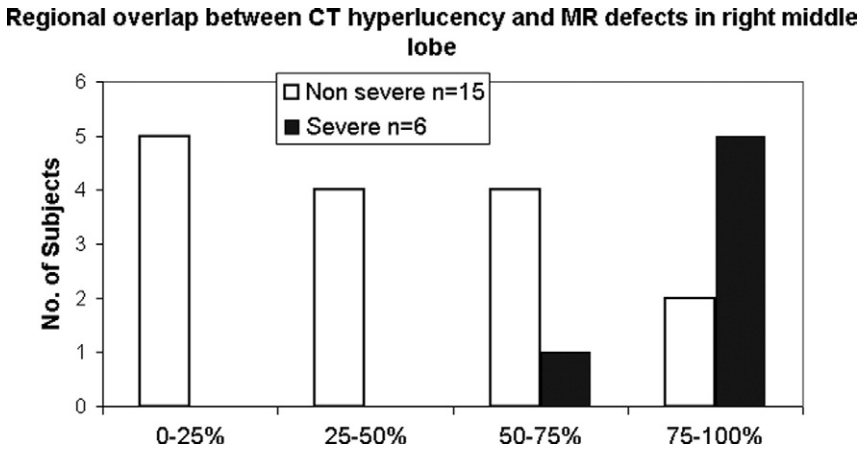

Figure 4. Qualitative distribution of regional overlap scores in the right middle lobe showing increased overlap between ventilation defects on hyperpolarized magnetic resonance imaging with hyperlucency on multidetector computed tomography for subjects with severe versus nonsevere asthma.

overlap between MR and MDCT. An additional limitation was that the bronchoscopic assessment of lobar defects was retrospective—lobes in *different* subjects were compared for differences in BAL inflammatory cell counts. Prospective studies using imaging to guide bronchoscopic assessment at both a defected lobe and non-defected lobe in the *same* subject are needed to verify the regional association of inflammation as compared with the possibility of diffuse inflammation throughout the lungs. However, the lack of a strong correlation between whole lung defect volume and inflammatory cell markers argues in favor of a stronger regional effect. Neutrophils are the cellular infiltrate found in acute episodes of asthma and in subclasses of patients with severe asthma; therefore, the presence of elevated neutrophil levels might be expected. However, it is somewhat surprising that in our analysis of the relationship between the structural changes and inflammatory pattern, eosinophils did not correlate with regions of defect or hyperlucency. It is unclear whether this is a result of the patient population or if ventilation defects on MRI manifest from a more acute inflammatory process. In addition, it is also of interest to compare large airway morphology, such as airway wall thickness and lumen area, as a function of defect burden. Although this is outside the scope of the present work, the tools to perform these measurements at specific airway bronchi are commercially available, and a careful analysis of these regional relationships is ongoing.

Noninvasive markers of obstructive lung disease are needed to characterize mechanisms and therapies in asthma and chronic obstructive pulmonary disease. Because of the observed spatial correspondence of abnormalities on MDCT and HP MRI, this work is also suggestive that regional hyperlucency on MDCT is a promising regional marker of airway obstruction that could provide a useful means to guide bronchoscopic assessment of the airways in ongoing mechanistic studies of asthma. At present, the MDCT imaging modality has advantages over HP MRI for image guidance studies, principally in its ability to depict both airway structure and regions of air trapping at FRC in three dimensions with high, nearly isotropic, spatial resolution. However, the ability of HP MRI to depict dynamic processes (26,27)is a key strength and new methods for three-dimensional dynamic hyperpolarized gas MRI are being introduced (7). These techniques provide spatial resolutions approaching that of CT in addition to information about respiratory dynamics at the level of the individual airways (28).

In conclusion, we have shown that established markers of obstructive lung disease correlate to obstructive physiology and that regional patterns of airway abnormality agree on MDCT and HP MRI. The increased neutrophils in BAL fluids sampled at locations of high ventilation defect suggest a regional association of inflammation and ventilation defects on MRI. However, prospective comparisons of image markers and cellular markers of inflammation using an image-guided bronchoscopic approach to sample multiple locations in the lungs of the same subject are necessary to confirm these results.

REFERENCES

1. Hartert TV, Peebles RS Jr. Epidemiology of asthma: the year in review. Curr Opin Pulm Med 2000; 6:4–9.
2. Sears MR, Greene JM, Willan AR, et al. A longitudinal, population-based, cohort study of childhood asthma followed to adulthood. N Engl J Med 2003; 349:1414–1422.
3. Postma DS, Timens W. Remodeling in asthma and chronic obstructive pulmonary disease. Proc Am Thorac Soc 2006; 3:434–439.
4. Permutt S. Current status of functional pulmonary imaging. Acad Radiol 2005; 12:1359–1361.
5. Haczku A, Emami K, Fischer MC, et al. Hyperpolarized 3He MRI in asthma measurements of regional ventilation following allergic sensitization and challenge in mice—preliminary results. Acad Radiol 2005; 12:1362–1370.
6. Holmes JH, Sorkness RL, Meibom SK, et al. Noninvasive mapping of regional response to segmental allergen challenge using magnetic resonance imaging and [F-18]fluorodeoxyglucose positron emission tomography. Magn Reson Med 2005; 53:1243–1250.
7. Holmes JH, Korosec FR, Du J, et al. Imaging of lung ventilation and respiratory dynamics in a single ventilation cycle using hyperpolarized He-3 MRI. J Magn Reson Imaging 2007; 26:630–636.
8. Newman KB, Lynch DA, Newman LS, et al. Quantitative computed tomography detects air trapping due to asthma. Chest 1994; 106:105–109.
9. Gono H, Fujimoto K, Kawakami S, et al. Evaluation of airway wall thickness and air trapping by HRCT in asymptomatic asthma. Eur Respir J 2003; 22:965–971.
10. Ueda T, Niimi A, Matsumoto H, et al. Role of small airways in asthma: investigation using high-resolution computed tomography. J Allergy Clin Immunol 2006; 118:1019–1025.
11. King GG, Eberl S, Salome CM, et al. Differences in airway closure between normal and asthmatic subjects measured with single-photon emission computed tomography and Technegas. Am J Respir Crit Care Med 1998; 158:1900–1906.
12. Harris RS, Winkler T, Tgavalekos N, et al. Regional pulmonary perfusion, inflation, and ventilation defects in bronchoconstricted patients with asthma. Am J Respir Crit Care Med 2006; 174:245–253.
13. Samee S, Altes T, Powers P, et al. Imaging the lungs in asthmatic patients by using hyperpolarized helium-3 magnetic resonance: assessment of response to methacholine and exercise challenge. J Allergy Clin Immunol 2003; 111:1205–1211.
14. de Lange EE, Altes TA, Patrie JT, et al. Evaluation of asthma with hyperpolarized helium-3 MRI: correlation with clinical severity and spirometry. Chest 2006; 130:1055–1062.
15. Hoffman EA, van Beek E. Hyperpolarized media MR imaging—expanding the boundaries? Acad Radiol 2006; 13:929–931.
16. de Lange EE, Altes TA, Patrie JT, et al. The variability of regional airflow obstruction within the lungs of patients with asthma: assessment with hyperpolarized helium-3 magnetic resonance imaging. J Allergy Clin Immunol 2007; 119:1072–1078.
17. Woodhouse N, Wild JM, Paley MN, et al. Combined helium-3/proton magnetic resonance imaging measurement of ventilated lung volumes in smokers compared to never-smokers. J Magn Reson Imaging 2005; 21:365–369.
18. NIH-NHLBI. Expert panel report: guidelines for the diagnosis and management of asthma. EPR-Update 2002 of NIH Publication 97-4051. Volume 2002: NIH/NHLBI; 2002.
19. Moore WC, Bleecker ER, Curran-Everett D, et al. Characterization of the severe asthma phenotype by the National Heart, Lung, and Blood Institute's Severe Asthma Research Program. J Allergy Clin Immunol 2007; 119:405–413.
20. Miller MR, Hankinson J, Brusasco V, et al. Standardisation of spirometry. Eur Respir J 2005; 26:319–338.
21. Wanger J, Clausen JL, Coates A, et al. Standardisation of the measurement of lung volumes. Eur Respir J 2005; 26:511–522.
22. Hankinson JL, Odencrantz JR, Fedan KB. Spirometric reference values from a sample of the general U.S. population. Am J Respir Crit Care Med 1999; 159:179–187.
23. Stocks J, Quanjer PH. Reference values for residual volume, functional residual capacity and total lung capacity. ATS Workshop on Lung Volume Measurements. Official Statement of The European Respiratory Society. Eur Respir J 1995; 8:492–506.
24. Lung function testing: selection of reference values and interpretative strategies. American Thoracic Society. Am Rev Respir Dis 1991;144:1202–1218.
25. Miller GW, Altes TA, Brookeman JR, et al. Hyperpolarized 3He lung ventilation imaging with B1-inhomogeneity correction in a single breath-hold scan. Magma 2004; 16:218–226.
26. Salerno M, Altes T, Brookeman J, et al. Dynamic spiral MRI of pulmonary gas flow using hyperpolarized ^{3}He: preliminary studies in healthy and diseased lungs. Magn Reson Med 2001; 46:667–677.
27. Wild J, Paley M, Kasuboski L, et al. Dynamic radial projection MRI of inhaled hyperpolarized ^{3}He gas. Magn Reson Med 2003; 49:991–997.
28. Holmes J, O'Halloran R, Brodsky E, et al. 3D Hyperpolarized He-3 MRI of ventilation using a multi-echo projection acquisition. Magn Reson Med. In press.